Temporal and spatial variations of shallow subsurface temperatue as a record of lateral variations in groundwater flow.

Bense, V.F.; Kooi, H.

published in
Journal of Geophysical Research. Solid Earth
2004

DOI (link to publisher)
10.1029/2003JB002782

document version
Publisher's PDF, also known as Version of record

Temporal and spatial variations of shallow subsurface temperature as a record of lateral variations in groundwater flow

V. F. Bense and H. Kooi

Department of Hydrology and Geo-Environmental Sciences, Faculty of Earth and Life Sciences, Vrije Universiteit Amsterdam, Amsterdam, Netherlands

Received 3 September 2003; revised 16 January 2004; accepted 4 February 2004; published 10 April 2004.

[1] In the present paper it is shown how profiles consisting of closely spaced ($\leq$10 m) temperature measurements at shallow depth, obtained at several instances during one season, provide a detailed record of lateral variations in vertical groundwater flow. This is illustrated by a field study around the Peel Boundary Fault zone that cuts through the unconsolidated, siliciclastic deposits that occur in the southeastern part of Netherlands. This regionally important fault forms at many locations a strong barrier to horizontal groundwater flow and therefore induces complex groundwater flow patterns. Temperature anomalies (over 2°C) are observed over short distances. These anomalies reverse over the season. Numerical modeling of coupled groundwater flow and heat transport demonstrates how the temporal and spatial variations of subsurface temperature are the result of the interaction between seasonal fluctuations in surface temperature and spatial variations in groundwater flow. In addition to the horizontal profiles, temperature-depth profiles obtained in groundwater observation wells were used to constrain the larger-scale characteristics of the groundwater flow system. In order to simulate the observed geothermal patterns it appeared to be essential to account for the long-term changes in surface temperature. Although groundwater temperature data are commonly used to constrain groundwater flow fields on regional scale or to calculate vertical groundwater velocities at point locations beneath small streams, the present study is one of the first to integrate these different scales and incorporate the impact of recent climate change. *INDEX TERMS:* 0999 Exploration Geophysics: General or miscellaneous; 1694 Global Change: Instruments and techniques; 1829 Hydrology: Groundwater hydrology; 1890 Hydrology: Wetlands; 1894 Hydrology: Instruments and techniques; *KEYWORDS:* geothermal methods, groundwater flow, fault zone, global warming, geological heterogeneity, heat flow

Citation: Bense, V. F., and H. Kooi (2004), Temporal and spatial variations of shallow subsurface temperature as a record of lateral variations in groundwater flow, *J. Geophys. Res.*, *109*, B04103, doi:10.1029/2003JB002782.

1. Introduction

[2] For many decades, subsurface temperature measurements have been used to constrain both relatively deep, regional groundwater flow systems [e.g., *Smith and Chapman*, 1983; *Forster and Smith*, 1989; *Mailloux et al.*, 1999; *Person et al.*, 1996; *Buttner and Huenges*, 2003] as well as more shallow, small-scale groundwater flow [e.g., *Andrews and Anderson*, 1979; *Bravo et al.*, 2002; *De Jong and Geirnaert*, 1979]. The key feature that is exploited to study these systems is that advection of heat by vertical upward or downward groundwater flow causes vertical temperature-depth profiles to become more convex or concave respectively, relative to the "undisturbed" geothermal gradient. Quantitative relationships developed by *Bredehoeft and Papadopulos* [1965], *Domenico and Palciauskas* [1973], and *Stallman* [1965] allow to estimate one-dimensional vertical flow rates from geothermal data. Additionally, *Lu and Ge* [1996] present a method to evaluate the temperature effects of horizontal groundwater flow in semi-confining layers.

[3] At shallow depths (<20 m), the interpretation of geothermal data is more complicated because seasonal changes in surface temperature tend to propagate to these depths. *Stallman* [1965] analyzed the exponential damping of surface amplitude and phase shift for groundwater flow and developed a type-curve method, which was subsequently applied and modified by other workers [e.g., *Boyle and Saleem*, 1979; *Cartwright*, 1979; *Taniguchi*, 1993]. Moreover, *Lapham* [1989] presented one-dimensional numerical simulations of the seasonally changing temperature regime at shallow depth to calculate vertical groundwater flow velocities under small streams.

[4] *Kukkonen and Clauser* [1994] and *Taniguchi et al.* [1999a, 1999b] show that, also at greater depth, temporal

0148-0227/04/2003JB002782$09.00

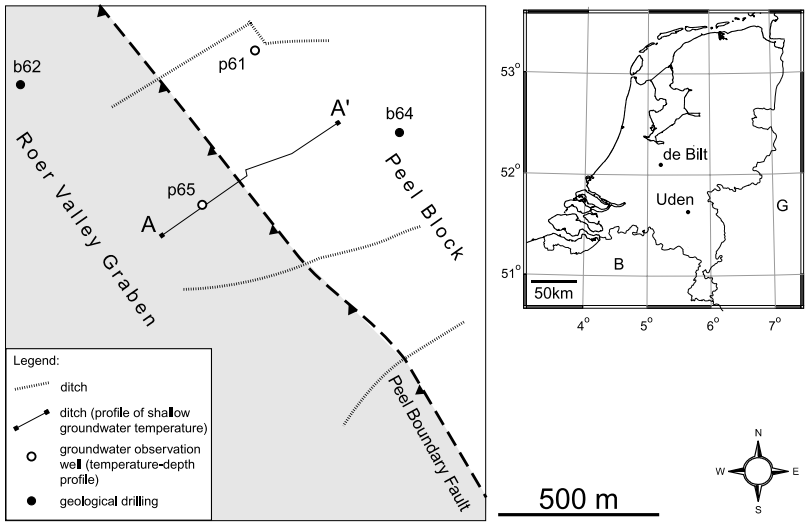

Figure 1. Location and simplified map of study area in the southeastern parts of Netherlands close to the village of Uden (*B* = Belgium, *G* = Germany). Location of boreholes that are used in this study are indicated.

changes in surface temperature can usually not be neglected in the interpretation of temperature-depth data for groundwater flow since climate change and changes in surface environmental conditions induce considerable curvature in temperature profiles up to depths of about 300 m. The effects of climate warming are globally recorded in the thermal regime and inversion techniques are widely applied to infer the rate and magnitudes of recent surface warming from temperature-depth profiles [e.g., *Huang et al.*, 2000; *Beltrami*, 2002].

[5] At very shallow depths (<0.5 m) diurnal temperature fluctuations dominate. Downward propagation of the diurnal heat wave is damped or enhanced by upward and downward flow in the same way as seasonal signals. Methods have been developed that combine measurements of surface temperature and of the temperature at shallow depth beneath small streams to monitor the rates of surface water-groundwater interaction at specific locations [e.g., *Ronan et al.*, 1998; *Constantz et al.*, 2002; *Silliman and Booth*, 1993]. *Csónka* [1968] and *Cartwright* [1974] have attempted to use shallow horizontal soil temperature profiles to discern areas of groundwater recharge and discharge, and *Krcmár and Mášín* [1970] reported to have mapped small faults based upon the seasonally changing pattern of soil temperature at a depth of 1.5 m. In spite of the great potential power and elegance of this technique, however, this work has had little impact. The significance of observed temperature patterns observed by *Cartwright* [1974] has remained obscure because large and non-trivial corrections had to be made for the presence of a vadose zone in the soil profile. *Csónka* [1968] obtained intriguing measurements in streams in Netherlands but he did not fully recognize the significance of his findings. Also, *Krcmár and Mášín* [1970] did not give a complete interpretation of the patterns they observed around shallow faults.

[6] Here, we revisit the approach of horizontal temperature profiling and demonstrate the full potential of the methodology. The field data that we present in this study were gathered in a wetland-like area around a shallow fault zone in the southeastern part of Netherlands. Repeated measurements have been done of the horizontal temperature profile below a ditch that runs perpendicular to the fault scarp. These measurements were done at a shallow depth (0.5 m) below the stream bottom by pushing a thermistor built into the tip of a plastic pole into the soil. We propose that the strong temperature anomalies (~2°C) that occur in these profiles are the result of the interaction between a seasonally fluctuating surface temperature and variations in groundwater flow velocities close to the surface. In order to test the validity of this interpretation, the observed horizontal temperature profiles are evaluated in the context of the larger scale hydrological system around the fault zone. Therefore, the observations from the horizontal temperature profiles are combined with temperature-depth data from groundwater observation wells and measurements of the electric conductivity of both groundwater samples and surface water. A numerical model was developed that incorporates both the interaction of a seasonally fluctuating surface temperature with shallow groundwater flow as well as the impact of groundwater flow on the subsurface temperature on a larger scale. Moreover, as suggested in other studies, for a correct interpretation of the deeper thermal regime it was essential to consider the effect of recent surface warming.

2. Site Description

[7] The field site discussed in this paper is located close to the village of Uden along the Peel Boundary Fault zone (PBFZ) (Figure 1) that is part of the regionally extending Roer Valley Rift System (RVRS) [*Michon et al.*, 2003; *Ziegler*, 1994]. At this location the PBFZ forms a small fault scarp with a height of ~3 m. Recent studies show that faults in the unconsolidated Quaternary and Tertiary sediments of the RVRS exert an important impact on the local and regional groundwater flow system [*Bense et al.*, 2003a; *Wallbraun*, 1992]. Faults in the RVRS generally impede groundwater movement while at the same location they can

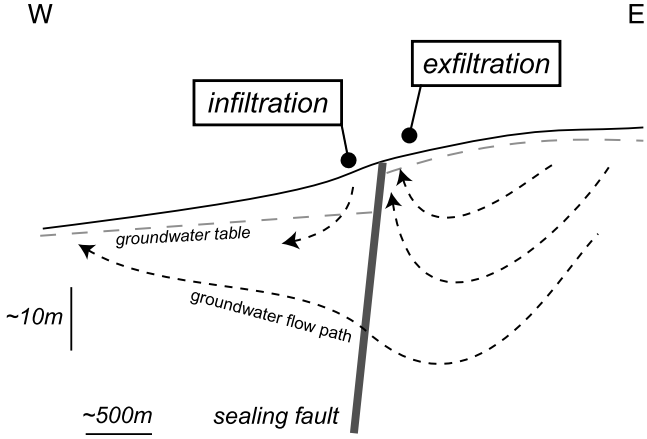

Figure 2. Schematic hydrological section showing the topographic driven groundwater flow pattern around the Peel Boundary Fault zone as inferred from water table measurements and regional hydraulic head data. A small wetland has developed just upstream of the fault where groundwater seepage occurs (exfiltration) as a result of the low permeability of the fault zone.

form the locus of focused pathways of vertical exchange of groundwater between otherwise separated aquifers. Outcrop studies carried out by *Bense et al.* [2003b] and *Lehner and Pilaar* [1997] show that clay smearing, particulate flow of grains and re-orientation of grains can explain the typical heterogeneous and anisotropic characteristics of fault zones in the RVRS. Moreover, these studies show that at shallow depth fault zones in the RVRS are generally limited to a width of less than ~10 m.

2.1. Geology

[8] The description of the geology of the field site is based upon two borings from either side of the PBFZ (b64 and b62; Figure 1). A top layer consisting of fine grained Quaternary aeolian sands is present on both sides of the fault. While in the Roer Valley Graben (RVG) this top unit has a thickness of ±20 m, on the Peel Block (PB) it is only a few meters thick. These fine sands are covering an aquifer that is built up of coarse to very coarse fluvial sands, of Quaternary age. On the PB a thick sequence of Miocene marine fine to very sand is found below the upper aquifer while in the RVG the main aquifer is underlain by a sequence of Quaternary fluvial clay, coarse sand and gravel.

2.2. Hydrology

[9] At many locations along the eastern side of the PBFZ small wetland-like areas have formed at places where very shallow groundwater tables occur even during the driest periods of the season. In observation well p61, situated in the PB, the hydraulic gradient indicates upward flow during the whole season. In contrast, in observation well p65, located in the topographically lower RVG, downward flow is inferred. Groundwater seepage is observed on the PB as strongly mineralized water flowing into ditches at localized spots.

[10] These upward flow and localized seepage phenomena on the higher parts on the PB and downward flow on the RVG are interpreted to be caused by the low permeability of the PBFZ (Figure 2). Aerial photographs show the heterogeneous nature of groundwater seepage in the distribution of wet and dry areas in fields where the bare soil is visible [*Bense et al.*, 2003a]. It is hypothesized that lithological heterogeneity in the cover layer on the PB causes the observed focused discharge of groundwater in discrete zones.

3. Methodology and Field Data

[11] Geothermal and geochemical data were gathered at the field site during a field campaign in the season 2002–2003. Temperature-depth profiles were measured in groundwater observation wells p61 and p65 (Figure 1) once a month. Both shallow groundwater temperature as well as the electric conductivity (EC) of the ditch water along A-A′ were routed three and two times respectively during the field campaign. Additionally, EC was measured of groundwater samples extracted from the filters in the two available groundwater observation wells.

3.1. Geothermal Data

[12] A winch with a thermistor probe attached on one end of a cable was used for measurements in the two observation wells (p61 and p65). Both wells have a diameter of 2.54 cm, which is small enough to minimize problems with instability of the water column through convective flow as a result of the temperature gradient present in the well [e.g., *Sammel*, 1968; *Cartwright*, 1979]. The instrument was fitted with a YSI Series 400 thermistor. The practical precision of the temperature measurements based on our field experience and the specified precision of the thermistor is in the order of 1×10^{-2} °C. The temperature sensing element was carefully lowered into the well in order to minimize a possible disruption of the original profile. In the top 25 m of the aquifer temperature was logged with intervals of 1 m, below this depth, each 2 m a temperature was logged. Figure 3 shows the time series of temperature-depth profiles that were obtained in wells p61 and p65.

[13] Measurement of temperatures below the ditch along A-A′ was carried out in March 2002, September 2002 and January 2003 (Figure 4a). Measurements were conducted with a plastic stick with a thermistor (YSI 400 series) built into its tip. This device is pushed into the ground so that the temperature at a desired depth can be measured after the temperature of the thermistor has stabilized. In this study, measurements were done at a depth of 50 cm below the bottom of the ditch. The limited strength of the stick did not allow us to probe to much greater depth. Measurements were done with a spacing of around 10 m. The ditch has typically only several centimeters of water.

[14] It can be shown based upon basic heat conduction theory [*Boyle and Saleem*, 1979; *Stallman*, 1965], that for conditions in Netherlands, diurnal temperature variation at a depth of 50 cm is less than ~0.4°C. Because acquisition of each temperature profile took several hours only (typically from around 10 A.M. to 2 P.M.) only a systematic trend in the profile may, therefore, be induced with a magnitude of ±0.1°C. The maximum error in temperature reading that could occur when the depth of measurement is inaccurate

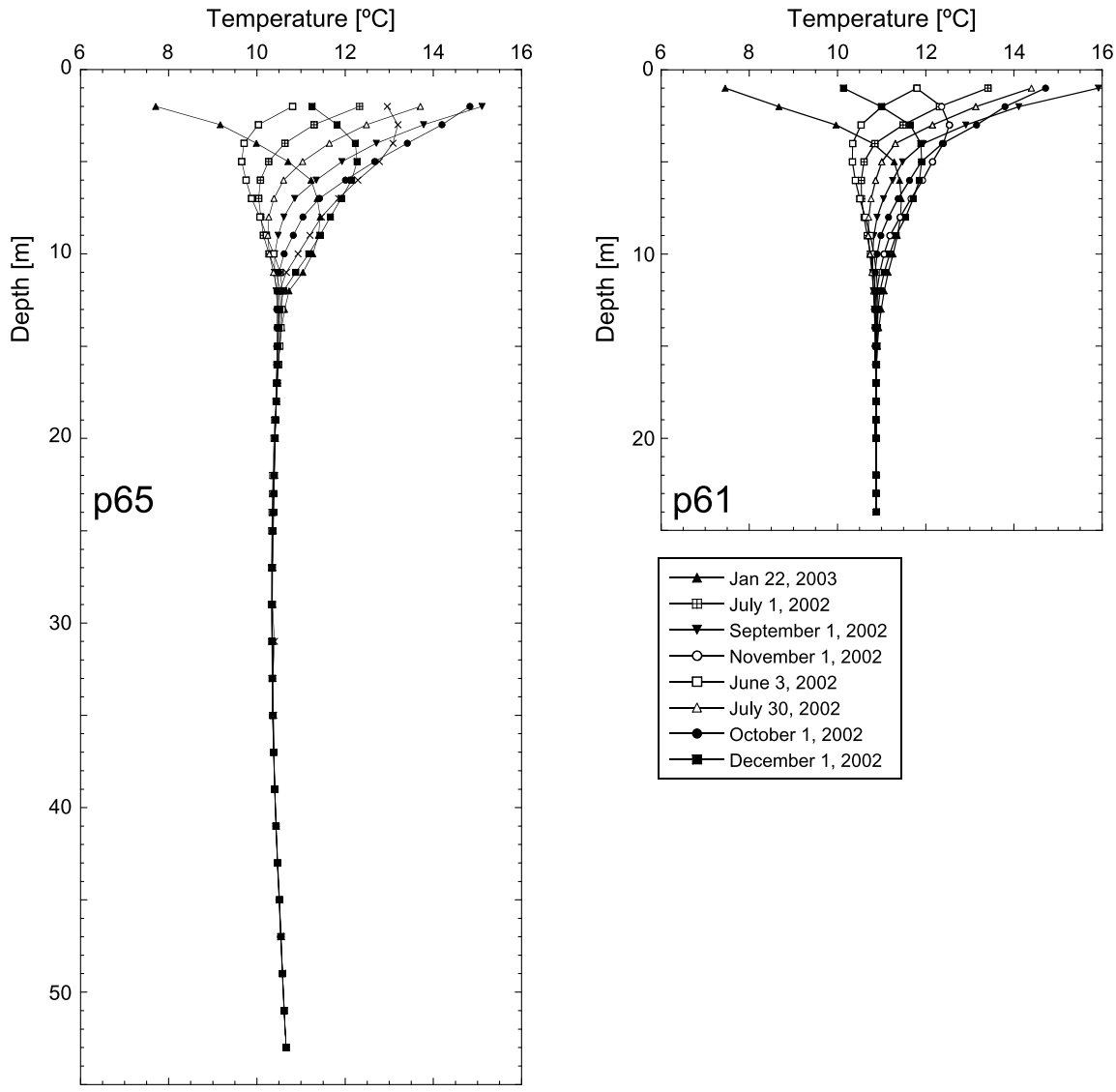

Figure 3. Observed temperature-depth profiles in wells p61 and p65 between May 2002 and January 2003. The upper ~15 m of the profiles show the impact of the seasonal fluctuation of surface temperature.

(i.e., when the measuring stick is pushed too deep or too shallow) is in the same range.

3.2. Electric Conductivity

[15] Measurements of EC were carried out using a simple field EC-meter with a precision of ±2 μS/cm. Next to the EC routing of the water in the ditch along A-A′, groundwater samples were taken from the two groundwater observation wells (p61 and p65) at three different depths (Table 1). To ascertain that the in situ groundwater at the depth of the filter was sampled, each well was pumped in advance until the total volume of the well had been flushed three times. Figure 4b presents the results of the EC measurements along A-A′.

4. Analysis of Individual Field Data

[16] In this section the field observations are first qualitatively described and analyzed individually as each data source holds a piece of information at a specific scale both spatially and temporally. Subsequently, we will show in the next section how these individual observations and their interpretation fit together into one model of coupled heat transport and groundwater flow around the PBFZ.

4.1. Temperature-Depth Profiles

[17] The impact of seasonal surface temperature variation is the most conspicuous feature of the temperature-depth profiles as depicted in Figure 3. Qualitative comparison of the temperature-depth profiles for well p65 and p61 first shows that the profiles in well p61 are vertically somewhat compressed compared to the profiles observed in well p65 (Figure 3). Moreover, the funnel-shaped envelope of the curves in the upper 15 m of the profiles appears to be slightly deflected to the right (higher temperatures). This suggests that the seasonally averaged temperature increases towards the surface. In order to be able to trace possible transient signals resulting from variations of mean surface

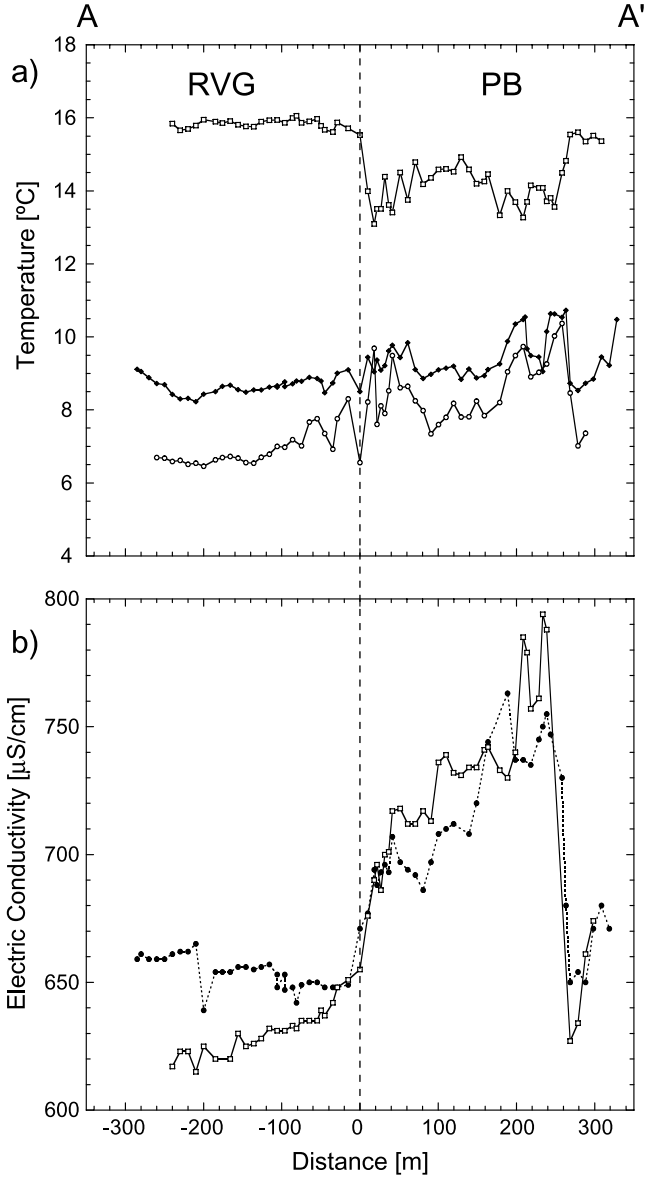

Figure 4. (a) Horizontal profiles of the soil temperature at a depth of 0.5 m below the ditch along section A-A′. (b) EC of the water in the ditch at the same locations in March (solid circle), September (square) and January (open circle). The vertical dashed line indicates the location of the PBFZ. The sites on the PB where strong temperature anomalies are observed largely correlate with patterns in the distribution of EC in the ditch, which suggests that at these locations discharge of relatively highly mineralized groundwater occurs.

temperature with a lower frequency than the annual cycle, the seasonal variation was filtered out in the following way. It is assumed that the amplitude of annual variation at a depth z can be described by a harmonic function [*Boyle and Saleem*, 1979; *Stallman*, 1965] stated as

$$T_z = \bar{T}_z + \Delta T_z \sin\left(\frac{2\pi t}{\tau} + b\right), \quad (1)$$

where b denotes the phase shift of the sine function. An optimizing routine was applied (Nelder-Mead Simplex method) to estimate values for $\bar{T}_z$, b and ΔT_z for each depth at which a time series of temperature was measured.

Table 1. Electric Conductivity of Groundwater Samples From Well p65 and p61

Sample	Depth, m below surface	EC, µS/cm
p65-1	3.5	463
p65-2	17	885
p65-3	54	357
p61-1	3	856
p61-2	15	697
p61-3	24	365

[18] Figure 5 displays the "corrected" temperature-depth profiles in wells p61 and p65. The typical "C"-shape of the profiles that is prominently present in both wells is observed in most parts of the world and generally attributed to global warming [*Beltrami*, 2002; *Huang et al.*, 2000; *Čermák et al.*, 1992; *Sebagenzi et al.*, 1992]. Small-amplitude wiggles are observed in the top ~10 m in Figure 5. As the profiles of well p61 and p65 show a similar trend with depth, these shallow wiggles are interpreted to be transient signals resulting from variations in annually averaged surface temperatures.

4.2. Horizontal Sections of Temperature and Electric Conductivity

[19] The horizontal temperature data that we gathered in the ditch along section A-A′ are shown in Figure 4a. Lateral temperature contrasts of over 2°C along A-A′ are observed

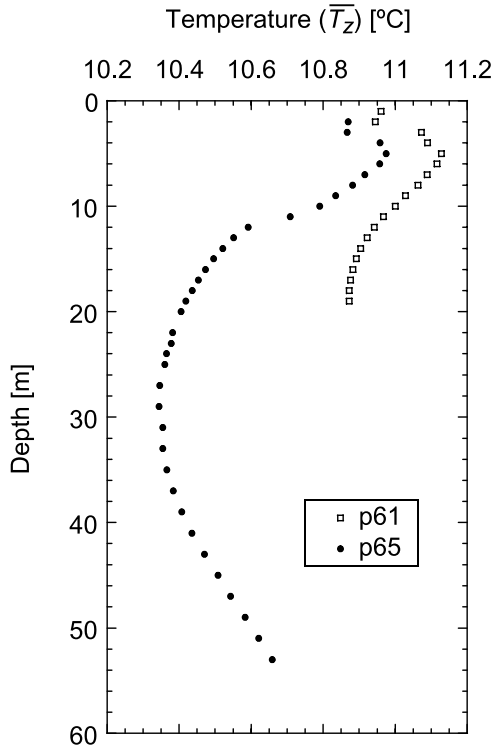

Figure 5. The average temperature-depth profiles ($\overline{T_z}$) over the period May 2002 and January 2003) as observed in wells p61 and p65. The annual variation in the upper part of the profiles has been removed by following the procedure as described in the text. The typical "C"-shape that these profiles show is found on a global scale and is attributed to surface warming over the last tens of years.

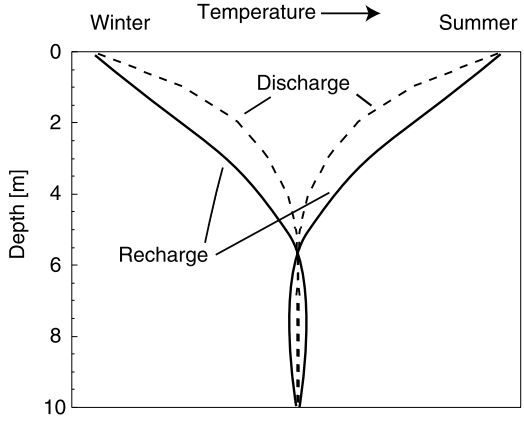

Figure 6. Qualitative sketch showing the difference in vertical temperature gradients between an area of exfiltration and infiltration during winter and summer. Relative small differences of the temperature gradient near the surface as a result of advective heat transport through vertical groundwater flow will result in significant temperature anomalies in horizontal profiles of groundwater temperature.

during both winter (January) and summer (September). Groundwater temperatures below the ditch on the RVG show far less lateral variation compared to the PB east of the PBFZ. Moreover, significant lateral variations exist in the amplitude of seasonal temperature variation at shallow depth. Especially on the hanging wall (RVG), seasonal temperature variations are notably larger than on the higher, and wetter areas upstream of the fault scarp. As a result, the temperatures on the PB are anomalously low compared to the lower lying areas during summer (September) while in winter time (January) groundwater temperatures in the wet areas on the PB are up to 2°C warmer. Figure 4 shows that the areas which show the least seasonal variation in temperature coincide with locations where relative strongly mineralized water (high EC) flows into the ditch, which suggests that these places are the locus of enhanced upward groundwater flow.

[20] Figure 6 shows how the observed temperature anomalies and their reversal from summer to winter can be qualitatively understood from the interaction between the seasonal temperature variation at the surface and the groundwater flow regime just below the ditch. In the top ~5 m of the sub-surface, vertical temperature gradients are very large compared to the background geothermal gradient. This is especially true during summer and winter. Infiltration and exfiltration of groundwater cause the vertical temperature profile to be deflected downward and upward, respectively, as a result of advection of heat [e.g., *Constantz et al.*, 2003] (Figure 6). Due to the high near-surface temperature gradient, relatively small lateral differences in infiltration or exfiltration rates can cause groundwater temperature close to the surface to vary considerably laterally. Comparison of the depicted temperature profiles for infiltration and exfiltration (Figure 6) demonstrates that during winter time a zone of exfiltrating groundwater causes a positive temperature anomaly, whereas in summer time a negative anomaly is produced. These reversals are apparent in the field observations (Figure 4a).

[21] The results of the EC routing carried out in March and September 2002 yield comparable patterns (Figure 4b). The EC of water in the ditch along A-A′ in the RVG averages around 600–650 μS/cm, while on the PB, the EC of the water in same ditch varies between 700–750 μS/cm. The fault scarp forms the abrupt boundary separating these two domains. A lower EC downstream is due to the fact that dissolved solids are rapidly precipitating (e.g., by oxidization) immediately after the discharging water reaches the surface. An even more pronounced contrast between the PB and RVG is found in the EC measurements of the groundwater samples from the shallow filters of wells p61 and p65 (Table 1). Mixing of high EC groundwater with surface water with a low EC smoothes the contrast between the PB and RVG in the ditch water. Therefore, the contrast between the PB and RVG section of the ditch is larger by the end of the summer (September) when the surface water contribution from upstream areas is relatively small.

5. Numerical Modeling

[22] In this section, the individual field data that are discussed above are brought together in a numerical simulation of the system. Therefore, the model was set-up to yield the general characteristics of the field site based upon reasonable parameter values. The model describes both the relatively small-scale phenomena associated with the interaction of shallow groundwater flow and seasonal temperature fluctuations close to the surface that are recorded in the horizontal profiles of temperature, and the deeper temperature data from the temperature-depth profiles that yield information on the larger-scale groundwater flow patterns. The aim of the model was to test the validity of the interpretations that we proposed in the latter section in a consistent framework. Therefore, we did not put much emphasis on optimization and calibration. The modeling was carried out using a generic finite element modeling tool (FlexPDE software, version 3.10, available from PDE Solutions Inc. at http://www.pdesolutions.com) that is used for the coupled solution of the governing equations.

[23] A 2-D vertical cross-sectional model was constructed along A-A′ in which a source term accounts for lateral inflow towards the ditch perpendicular to the model section. The latter occurs because the ditch is draining and recharging below and above the fault, respectively. Figure 7 shows part of the complete model domain that is 1250 m long and 400 m high. Groundwater flow in the sectional model is kept in quasi steady state, only varying over time as a result of the temperature dependency of K. Observed hydraulic head gradients show little variation over the season in these areas with shallow groundwater tables. Therefore, for simplicity, the hydraulic boundary conditions are kept constant. The temperature regime is transient as both the seasonal fluctuation of temperature at the surface and the longer term annual variation of the mean surface temperature are implemented.

5.1. Groundwater Flow

[24] The following equation is used to model steady state flow in the model section (unit thickness):

$$\nabla \cdot \vec{q} + q_{lat} = 0, \tag{2}$$

where q_{lat} is the two-sided (total) lateral inflow perpendicular to the section. The nabla operator (∇) applies to the 2-D section only.

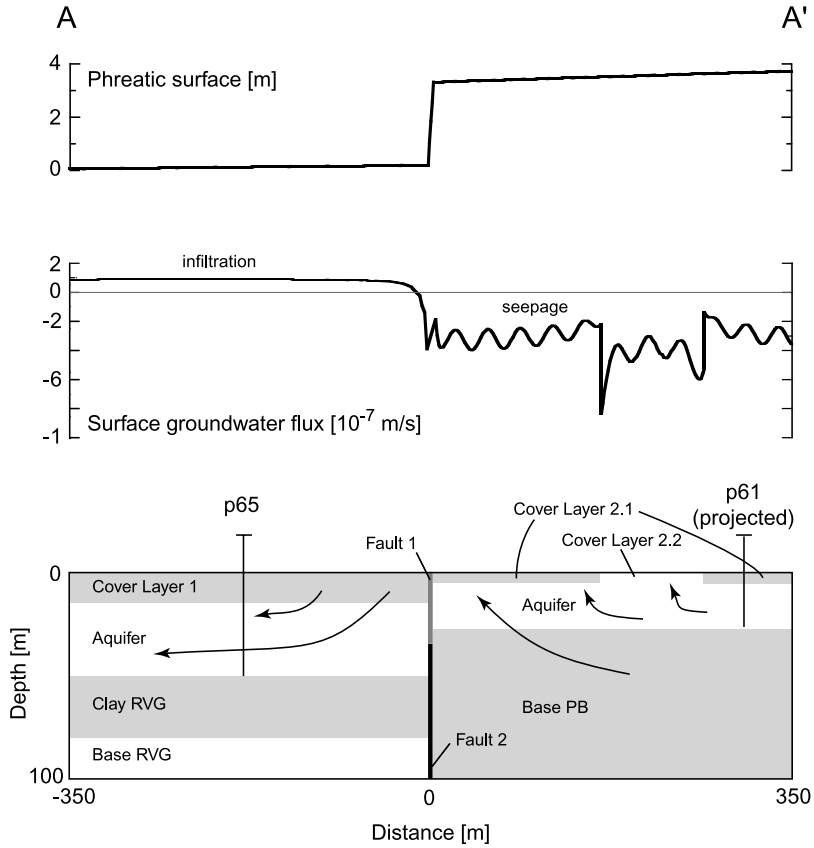

Figure 7. Hydrogeological cross section over the PBFZ along A-A′ showing the groundwater flow patterns in the model, the phreatic groundwater level (the upper boundary condition of the numerical simulation) and the resulting groundwater flux at the surface.

[25] Groundwater flow is towards the ditch on the PB, draining the underlying aquifer and away from the ditch (recharging the aquifer) in the RVG. Therefore, two different values, $q_{lat,PB}$ and $q_{lat,RVG}$, were defined for the PB and RVG, respectively.

[26] Darcy's Law is implemented as

$$\vec{q} = -K\nabla h, \tag{3}$$

where hydraulic conductivity is defined as $K = k\frac{\rho_f g}{\mu}$. We explicitly take into account the temperature dependency of μ. Values of μ and, hence, K vary by a factor of two in the model because near surface groundwater temperature ranges from about 3 to 18. Although ρ_f also in a function of T, the temperature effect on ρ_f in the same temperature range is only ~2‰.

[27] Hydraulic head is fixed at the top of the model following the hydraulic gradients that were measured in earlier studies [*Bense et al.*, 2003a; *Stuurman and Atari*, 1997] (upper panel in Figure 7). The left- and right-hand side of the model domain are constant head boundaries with a value in accordance with the upper boundary condition so that over the left and right boundaries flow is horizontal.

[28] Table 2 summarizes the hydraulic properties of the units, as used in he simulations. Only a few direct field measurements of the hydraulic properties of the different hydrogeological units are available for the study area. Here we use parameter values that were compiled from earlier studies [*Bense et al.*, 2003a]. The top layer on the PB is assigned an heterogeneous permeability distribution using a sine-function distribution ($k = 2.9 \times 10^{-12}$ m^2 to 4.8×10^{-12} m^2). A zone of higher permeability ($k = 1.2 \times 10^{-11}$ m^2 to 1.9×10^{-11} m^2) is modeled within the top layer. The amount of heterogeneity in the top layer of our model on the PB is regarded to be reasonable as it is in the same range as reported by *Bierkens* [1994] based upon laboratory measurements on similar sediments. The fault zone is schematized as a 5-m wide zone of low permeability with a resistance r which is defined as w/K. The upper ($z < 30$ m) and lower part of the PBFZ are assigned values of r_1 (Fault 1) and r_2 (Fault 2), respectively. This distinction has been made because it is likely that the resistance of the PBFZ significantly increases

Table 2. Permeability (k) Values Used in the Numerical Simulation[a]

Unit	Description	Permeability (k)
Aquifer	coarse sand	$4.62 \cdot 10^{-11}$
Cover layer 1	fine sand - aeolian	$1.5 \cdot 10^{-11}$
Cover layer 2.1	fine sand - aeolian	$2.9–4.8 \cdot 10^{-12}$
Cover layer 2.2	medium sand	$1.2–1.9 \cdot 10^{-11}$
Clay RVG	clay	$1.5 \cdot 10^{-16}$
Base RVG	sand	$1.5 \cdot 10^{-11}$
Base PB	fine sand - marine	$2 \cdot 10^{-12}$
Fault 1	mixture of clay sand	$7.7 \cdot 10^{-14}$
Fault 2	mixture of clay sand	$2.7 \cdot 10^{-15}$

[a]Unit names refer to Figure 7.

with depth. The borehole records for b64 and b62 (Figure 1) show that no clay is present in the upper part of the stratigraphy which makes it unlikely that in the upper part ($z < 30$ m) of the system clay smearing has occurred along the fault plane. *Bense et al.* [2003a] show that r_1 can be estimated as ~100 days based upon an analysis of hydraulic head gradients on either side of the fault which is the value that is used in the present study.

5.2. Heat Transport

[29] The following equation is used for the simultaneous transfer of heat and fluid through heat conduction and advection in an isotropic and homogeneous medium [e.g., *Stallman*, 1960]:

$$c\rho\frac{\partial T}{\partial t} + c_w\rho_w\vec{q}\nabla T + c_w\rho_w T_{lat}q_{lat} - \kappa\nabla^2 T = 0, \qquad (4)$$

in which the term $c_w\rho_w T_{lat}q_{lat}$ is an extra source term to the standard equation in order to account for the lateral inflow (advection) of heat perpendicular to the modeled section as a result of the lateral flow of water towards/from the ditch. The operators ∇ and ∇^2 apply to the 2-D section only.

[30] At the base of the model domain (z = 400 m) temperature is fixed at 20, following a geothermal gradient of ~25 °C^{-1} km^{-1}, which is in accordance with values recorded in deeper wells [*Stolk*, 2000]. This gradient corresponds to a heat flow of $2.5 \times 0.025 = 62.5$ mW m^{-2} for κ = 2.5 Jm^{-1} s^{-1} °C^{-1} which is in reasonable agreement with published heat flow data for Netherlands [e.g., *Van Balen et al.*, 2002]. The left and right sides of the model domain were assigned a linear thermal gradient. The temperature of the water in- or outflowing perpendicular to the section (q_{lat}) is assumed to equal the temperature in the section so that $T_{lat} \approx T$. Hence, the effects of possible heat conduction perpendicular to the section is not taken into account in the present model.

[31] The distribution of thermal properties in the model was assumed to be homogeneous. Representative values for these sediments were used as given by *De Jong and Geirnaert* [1979] and subsequently *Stolk* [2000] which yield κ = 2.5 W °C^{-1} m^{-1}, c = 2013 Jkg^{-1} °C^{-1}, ρ = 2105 kg m^{-3}.

5.3. Modeling Strategy

[32] Transient model calculations start for the year 1900. Initial conditions are obtained by calculating a stationary temperature field using a surface temperature representative for the year 1900 based upon the available meteorological record of air temperature at De Bilt meteorological station (Figure 8). Subsequently the surface temperature is allowed to increase following the trend in mean annual air temperature up to the year 1960. Proceeding from that date, the history of the annual average temperature ($\bar{T}$) is used in a stepwise manner to forward calculate the temperature field up to the year 2000. Surface temperature (T_s) for the year 2001 and 2002 is represented by a sine-function:

$$T_s = \bar{T} + \Delta T_s \sin 2\pi/\tau, \qquad (5)$$

in which ΔT_s was chosen in agreement with observed meteorological data from De Bilt meteorological station.

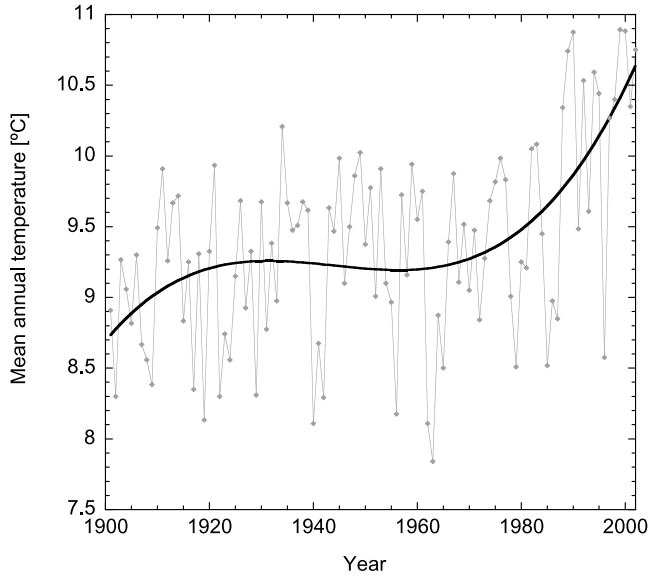

Figure 8. The mean annual air temperature as recorded at the De Bilt meteorological station (see Figure 1 for location). The solid line is a polynomal fit of the data. Up to the year 1960 this trend line is used to mimic surface temperature in the numerical model. Thereafter, the actual mean annual temperatures are used to constrain the simulation of the temperature field around the PBFZ.

[33] The values of permeability and thermal properties of the hydrogeologic units were fixed in the model. Only the values for $q_{lat,PB}$ and $q_{lat,RVG}$ were optimized using "trial and error" by visual comparison between observed and simulated temperatures. No simultaneous optimization of both temperature data and hydraulic heads has been carried out as was demonstrated by, for example, *Woodbury and Smith* [1988] or *Bravo et al.* [2002]. The middle panel in Figure 7 shows the distribution of groundwater flow velocities at the surface. A simple analysis taking into account the local configuration of the groundwater table of the area and the transmissivity of the underlying aquifer (the product of a vertically averaged K and thickness of the aquifer) showed that the optimized values of lateral in- and outflow in the 2-D section are reasonable estimates.

6. Results and Discussion

[34] The upper panel in Figure 9 shows the initial steady state temperature distribution for the year 1900. Upward groundwater flow on the PB as a result of the low-permeable fault zone causes the temperatures to be higher there than at the same depth in the RVG. The lower panel in Figure 9 shows the calculated temperature distribution for the year 2002 in the absence of seasonal annual variations of surface temperature. As a result of surface warming over the last century, the thermal contrast between discharge area and recharge area has dramatically reduced.

[35] In order to be able to compare the field data to the simulation results, observation well p61 is projected onto A-A′. Since well p61 is located along the ditch north of A-A′ (Figure 1), it is assumed that similar groundwater flow

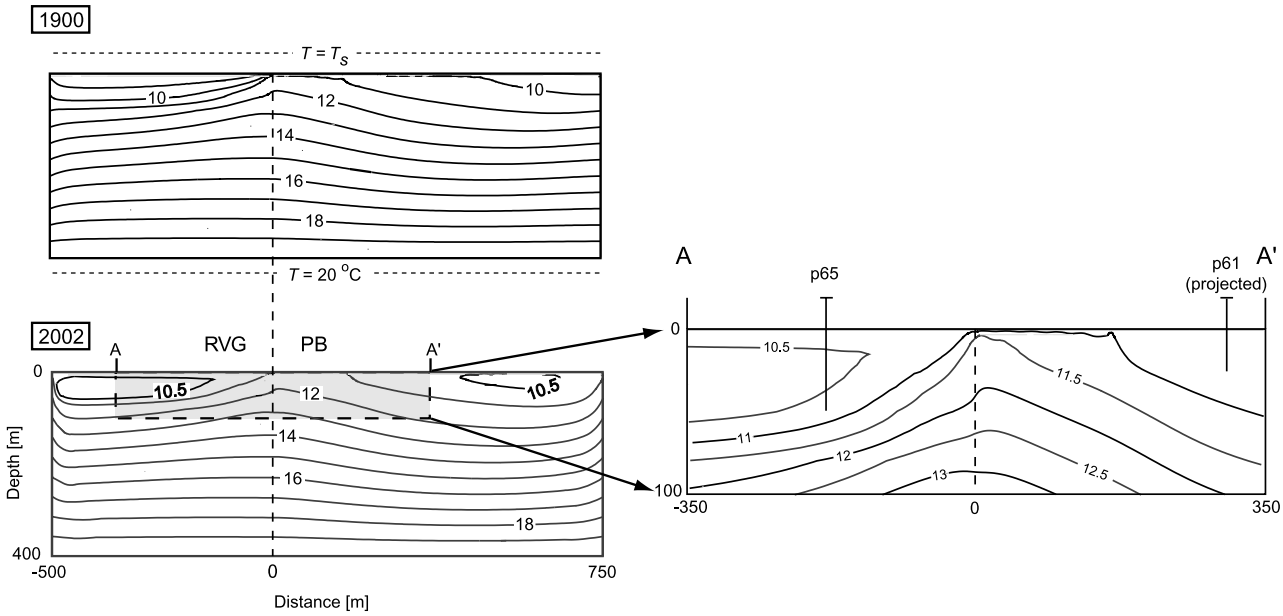

Figure 9. Temperature distribution (isotherms are labeled in °C) in the absence of seasonal temperature variation at the surface as calculated for the years 1900 and 2002 for the entire model domain. The PBFZ is located along the dashed line. The shaded area indicates the extent of the cross section shown in Figure 7.

conditions are met at well p61 as around the ditch along A-A′ at the same distance from the fault scarp.

[36] Comparison with the field data (Figure 10) shows that the shape of the deeper observed temperature-depth profiles can be reasonably well explained by a net increase in mean annual surface temperature as recorded in the meteorological record from De Bilt in combination with the estimated rates of groundwater flow in the system. However, it appears that the temperature in the upper part of the system is generally higher (several tenths of a °C) than the model prediction. This effect is stronger for the discharge area (p61) than for the recharge area (p65). As the signal of the seasonal variations largely overprints these deviations, results improve when the seasonally fluctuating surface temperature is implemented in the simulation. The amplitude and damping with depth of the simulated temperature-depth profiles compare well to the observed data from well p61 and p65 (Figure 11).

[37] Several reasons can be considered for the observed differences between calculated and observed temperatures at shallow depth (<10 m). First, De Bilt meteorological station is located at ~50 km lateral distance from the field site where the mean annual surface temperature is not necessary representative for that around the village of Uden. However, based upon an inspection of maps of regional variation of mean annual temperatures in Netherlands at the Royal Meteorological Institute of Netherlands, this effect must be of minor impact. Probably of more importance is the effect that there can exist a significant difference between the air temperature as documented in meteorological records and the soil temperature as recorded in the geothermal record [e.g., *Putnam and Chapman*, 1996; *Beltrami*, 2001]. Several studies have shown that changes in either vegetation cover or groundwater depth can significantly impact soil temperature [*Lewis and Wang*, 1998; *Taniguchi et al.*, 1999b]. Another effect is that groundwater flow will become transient if for example the intensities of groundwater seepage and recharge differ significantly between winter and summer, which will induce additional disturbances of the geothermal regime. Moreover, in case the surface temperature is significantly

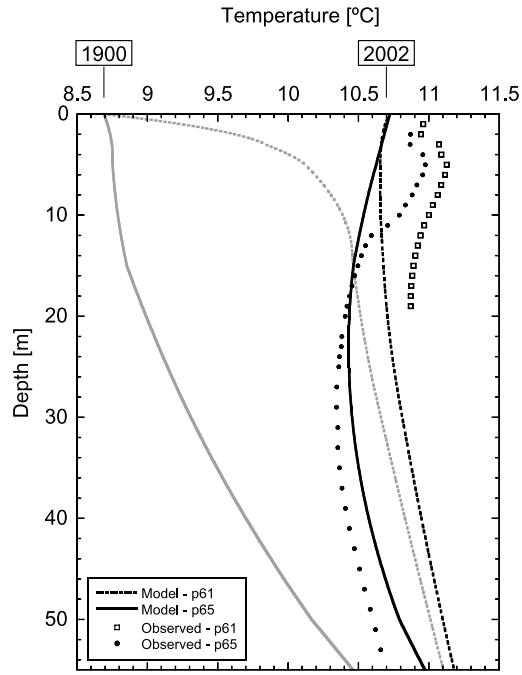

Figure 10. A comparison of the observed temperature-depth profiles with the results of the simulation shows that in the upper part of the profiles the simulated temperatures are too low relative to the observed patterns. Several reasons to explain this discrepancy are discussed in the text.

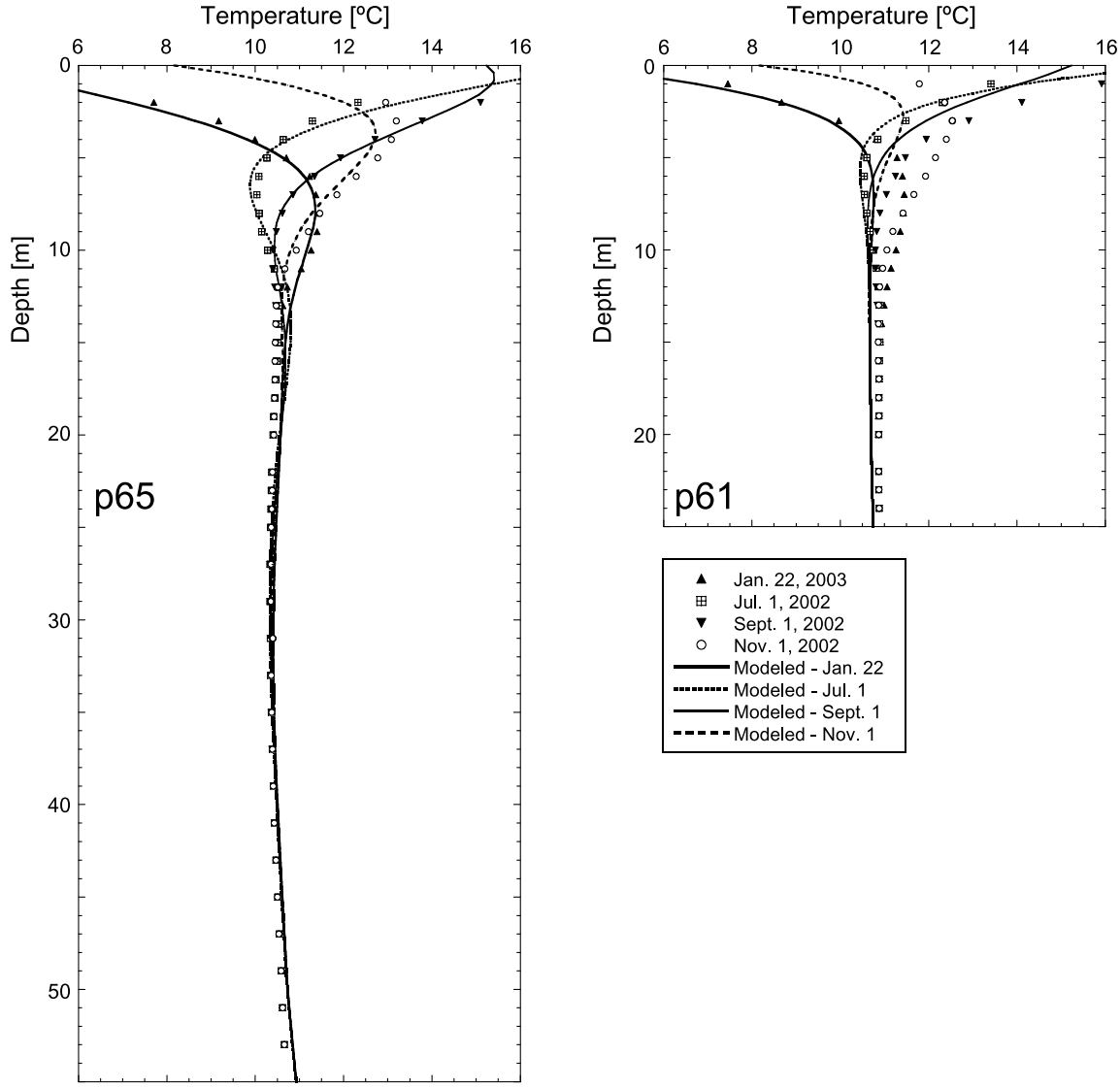

Figure 11. Model to data comparison of temperature-depth profiles in which the seasonal surface temperature variation is included. The seasonally fluctuating surface temperature is mimicked using a sine-function with amplitude, mean and phase-shift in accordance with observations at De Bilt meteorological station.

different from the sine function that is applied in the simulation, if for example during periods of snow cover temperature is fixed at 0°C deviations between simulated and observed temperatures can be expected [*Lapham*, 1989]. The present model does not include any of these processes that possibly explain the observed misfits in the upper part of the profiles because groundwater flow is kept steady state over the season, the aquifer is assumed to be saturated, local effects of vegetation cover are not considered and the surface temperature is simulated as to vary sinusoidally over the season.

[38] The synthetic sections of horizontal soil temperature at a depth of 50 cm show the same inversion over the season as observed in the field data set, which supports our initial analysis of the observed patterns (Figure 12). As the thermal properties in the model are uniform, the simulated temperature patterns are solely the result of differences in vertical groundwater flow close to the surface (Figure 7). In reality, the thermal properties of the aquifer will slightly vary laterally. Preliminary modeling results show that, in case of extreme, unrealistic, lateral contrasts of the thermal conductivity of the cover layer (κ = 1 to 4 W °C^{-1} m^{-1}), these variations can be reflected in temperature anomalies with a comparable magnitude as observed around the PBFZ. However, the sediments around the PBFZ are believed to be relatively homogeneous and since a strong correlation between EC anomalies and shallow temperature patterns was observed it is argued that the observed temperature anomalies close to the surface are mainly caused by differences in vertical groundwater flow.

[39] We have avoided interpretation problems arising from the presence of a vadose zone in the soil profile as described by *Cartwright* [1974] because we did measurements of horizontal temperature profiles in saturated sediments below a ditch. However, the depth at which measurements are carried out with the described method

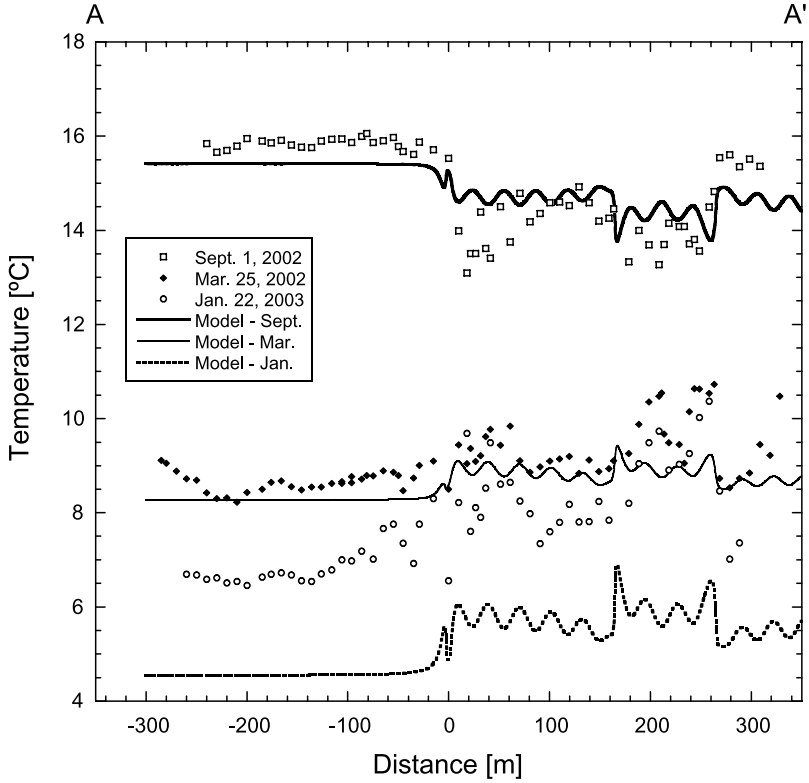

Figure 12. Model to data comparison of the horizontal temperature profiles along A-A′ at a depth of 50 cm below the surface. The heterogeneity of the groundwater flow field can reasonably explain the observed temperature anomalies and their reversal over the season.

of horizontal profiling is of considerable importance. Figure 6 illustrates that the amplitude of temperature anomalies due to the interaction of lateral variations in groundwater flow and seasonal surface temperature change increase in the first meters below ground surface and that an optimal depth of measurement exists. Ideally, measurements should just reflect the interaction between seasonal surface temperature changes and groundwater flow without complications by temperature signals associated with diurnal surface temperature changes. Measurement at relatively large depth has the additional advantage that relatively short-term surface temperature variations that are superimposed on the seasonal signal are largely damped. In the current study, the employed measurement depth of 0.5 m apparently sufficed to bring out anomalies that are the result of interaction between groundwater flow and seasonal temperature change. These considerations are useful in choosing an appropriate depth of measurement in a field campaign. Detailed meteorological records, rather than representing surface temperature by a simple sine function, may be incorporated in numerical modeling to refine the interpretation of seepage and infiltration rates.

7. Conclusion

[40] The geothermal regime around a shallow fault zone in Netherlands was simulated by incorporating into one model both a seasonally fluctuating surface temperature as well as the longer term surface warming over the last century. The presence of a low-permeable fault zone is needed to explain the occurrence of groundwater discharge (seepage) on the topographically higher areas while groundwater recharge (infiltration) is observed in the topographic lower areas downstream of the fault scarp. The present study shows how complex transient geothermal patterns at shallow depth in this system can be understood by coupling transient heat transport to steady state groundwater flow. We have shown that for a correct simulation of the observed geothermal patterns at larger depth it is essential to incorporate the impact of recent surface warming in the numerical model. Constraining the simulation with observed meteorological data showed that there is a significant discrepancy between air temperature and the ground surface temperature that is recorded in the geothermal regime, a finding which has been reported in other studies.

[41] In the present study it is shown that subtle variations in groundwater flow velocities ($\sim$2 to 4 $\times$ 10^{-7} m^{-1} s^{-1}) close to the surface result in significant ($\sim$0.5°C) temperature anomalies as a result of the interaction of seasonal surface temperature variation and groundwater flow. Therefore, horizontal profiles of shallow groundwater temperature are a promising tool to asses the small-scale heterogeneity of surface-groundwater interaction which is a key issue in for example wetland research [e.g., *Bravo et al.*, 2002; *Hunt et al.*, 1997, 1998] and more general hydrologic studies concerning the estimation of water budgets, groundwater recharge and groundwater quality [e.g., *Silliman et al.*, 1995]. A field method based upon this mechanism provides an important extension to existing methods since shallow horizontal temperature profiling can be used, unlike the other available methodologies that rely on elaborate field instrumentation at selected sites, to carry out extensive

regional mapping in large detail. Such an approach may, therefore, be employed in the prospecting of key zones of groundwater discharge or recharge that are so essential to the management of a variety of groundwater systems that are dominated by hydrogeological heterogeneity and associated preferential flow of groundwater and dissolved contaminants or nutrients.

Notation

$\vec{q}$ Darcy velocity, m s^{-1};
h hydraulic head, m;
T temperature, °C;
T_s temperature at the surface, °C;
$\overline{T}_z$ average temperature at depth z, °C;
ΔT_z amplitude of seasonal temperature variation at depth z, °C;
k permeability, m^2;
K hydraulic conductivity, m s^{-1};
z depth, m;
κ thermal conductivity, W $°C^{-1}$ m^{-1};
c specific heat of saturated aquifer, Jkg^{-1} $°C^{-1}$;
c_w specific heat of water, Jkg^{-1} $°C^{-1}$;
ρ density of saturated aquifer, kg m^{-3};
ρ_w density of water, kg m^{-3};
τ duration of one year, second;
r fault zone resistance, days;
w fault zone width, meter.

[42] **Acknowledgments.** Elmer van den Berg, Vincent Post, and Boris van Breukelen are gratefully acknowledged for their help during the field campaigns. Ronald van Balen and Gualbert Oude Essink are thanked for critical comments on an earlier version of the manuscript. We thank Mark Person, Volker Rath, and Associate Editor Adrian Lenardic for their thoughtful reviews of the original manuscript. This is publication 2004.01.05 of Netherlands Research School of Sedimentary Geology.

References

Andrews, C. B., and M. P. Anderson (1979), Thermal alteration of groundater caused by seepage from a cooling lake, *Water Resour. Res.*, *15*, 595–602.

Beltrami, H. (2001), On the relationship between ground temperature histories and meteorological records: A report on the Pomquet station, *Global Planet. Change*, *29*, 327–348.

Beltrami, H. (2002), Earth's long-term memory, *Science*, *297*, 206–207.

Bense, V. F., R. T. Van Balen, and J. J. De Vries (2003a), The impact of faults on the hydrogeological conditions in the Roer Valley Rift System: An overview, *Geol. Mijnbouw*, *82*, 41–53.

Bense, V. F., E. H. Van den Berg, and R. T. Van Balen (2003b), Deformation mechanisms and hydraulic properties of fault zones in unconsolidated sediments: The Roer Valley Rift System, the Netherlands, *Hydrogeol. J.*, *11*, 319–332.

Bierkens, M. F. P. (1994), Complex confining layers: A stochastic analysis of hydraulic properties at various scales, Ph.D. thesis, Univ. Utrecht, Utrecht, Netherlands.

Boyle, J. M., and Z. A. Saleem (1979), Determination of recharge rates using temperature-depth profiles in wells, *Water Resour. Res.*, *15*, 1616–1622.

Bravo, H. R., F. Jiang, and R. J. Hunt (2002), Using groundwater temperature data to constrain parameter estimation in a groundwater flow model, *Water Resour. Res.*, *38*(8), 1153, doi:10.1029/2000WR000172.

Bredehoeft, J. D., and I. S. Papadopulos (1965), Rates of vertical groundwater movement estimated from the Earth's thermal profile, *Water Resour. Res.*, *1*, 325–328.

Buttner, G., and E. Huenges (2003), The heat transfer in the region of the Mauna Kea (Hawaii)—Constraints from borehole temperature measurements and coupled thermo-hydraulic modeling, *Tectonophysics*, *371*, 23–40.

Cartwright, K. (1974), Tracing shallow groundwater systems by soil temperatures, *Water Resour. Res.*, *10*, 847–855.

Cartwright, K. (1979), Measurement of fluid velocity using temperature profiles: Experimental verification, *J. Hydrol.*, *43*, 185–194.

Čermák, V., L. Bodri, and J. Šafanda (1992), Recent climate change recorded in the underground: Evidence from Cuba, *Palaeogeogr. Palaeoclimatol. Palaeoecol.*, *98*, 219–223.

Constantz, J., A. E. Stewart, R. Niswonger, and L. Sarma (2002), Analysis of temperature profiles for investigating stream losses beneath ephemeral channels, *Water Resour. Res.*, *38*(12), 1316, doi:10.1029/2001WR001221.

Constantz, J., S. W. Tyler, and K. Edward (2003), Temperature-profile methods for estimating percolation rates in arid environments, *Vadose Zone J.*, *2*, 12–24.

Csónka, J. (1968), Report on the applicability of the geothermal method in the Netherlands (in Dutch), *Tech. Rep. OS 92-40A*, TNO Dienst Grondwaterverkenning, Delft, Netherlands.

De Jong, S. J., and W. Geirnaert (1979), The groundwater thermal regime in the Flevo polders and the Gelderse Vallei (southern IJsselmeer area The Netherlands), *Geol. Mijnbouw*, *58*, 295–304.

Domenico, P. A., and V. V. Palciauskas (1973), Theoretical analysis of forced convective heat transfer in regional ground-water flow, *Geol. Soc. Am. Bull.*, *84*, 3803–3813.

Forster, C., and L. Smith (1989), The influence of groundwater flow on thermal regimes in mountaineous terrain: A model study, *J. Geophys. Res.*, *94*, 9439–9451.

Huang, S., H. N. Pollack, and P.-Y. Shen (2000), Temperature trends over the past five centuries reconstructed from borehole temperatures, *Nature*, *403*, 756–758.

Hunt, R. J., D. P. Krabbenhoft, and M. P. Anderson (1997), Assessing hydrogeochemical heterogeneity in natural and constructed wetlands, *Biogeochemistry*, *39*, 271–293.

Hunt, R. J., T. D. Bullen, D. P. Krabbenhoft, and C. Kendall (1998), Using stable isotopes of water and Strontium to investigate the hydrology of a natural and a constructed wetland, *Ground Water*, *36*, 434–443.

Krcmár, B., and J. Mášín (1970), Prospecting by the geothermic method, *Geophys. Prospect.*, *18*, 255–260.

Kukkonen, I. T., and C. Clauser (1994), Simulation of heat transfer at the Kola deep-hole site: Implications for advection, heat refraction and paleoclimate effects, *Geophysics J. Int.*, *116*, 409–420.

Lapham, W. W. (1989), Use of temperature profiles beneath streams to determine rates of vertical ground-water flow and vertical hydraulic conductivity, *U.S. Geol. Surv. Water Supply Pap.*, 2337.

Lehner, F. K., and W. F. Pilaar (1997), On a mechanism of clay smear emplacement in synsedimentary normal faults, in *Hydrocarbon Seals: Importance for Exploration and Production*, vol. 7, *NPF Spec. Publ.*, edited by P. Møller-Pedersen and A. G. Koestler, pp. 39–50, Elsevier Sci., New York.

Lewis, T. J., and L. Wang (1998), Geothermal evidence for deforestation induced warming: Implications for the climatic development, *Geophys. Res. Lett.*, *25*, 535–538.

Lu, N., and S. Ge (1996), Effect of horizontal heat and fluid flow on the vertical temperature distribution in a semiconfining layer, *Water Resour. Res.*, *32*, 1449–1453.

Mailloux, B. J., M. Person, S. Kelley, N. Dunbar, S. Cather, L. Strayer, and P. Hudleston (1999), Tectonic controls on the hydrogeology of the Rio Grande Rift, New Mexico, *Water Resour. Res.*, *35*, 2641–2659.

Michon, L., R. T. Van Balen, O. Merle, and H. Pagnier (2003), The Cenozoic evolution of the Roer Valley Rift System integrated at a European scale, *Tectonophysics*, *367*, 101–126.

Person, M., J. P. Raffensberger, S. Ge, and G. Garven (1996), Basin-scale hydrogeologic modeling, *Rev. Geophys.*, *34*, 61–87.

Putnam, S. N., and D. S. Chapman (1996), A geothermal climate change observatory: First year results from Emigrant Pass in northwest Utah, *J. Geophys. Res.*, *101*, 21,877–21,890.

Ronan, A. D., D. E. Prudic, C. E. Thodal, and J. Constantz (1998), Field study and simulation and diurnal temperature effects on infiltration and variably saturated flow beneath an ephemeral stream, *Water Resour. Res.*, *34*, 2137–2153.

Sammel, E. A. (1968), Convective flow and its effect on temperature logging in small-diameter wells, *Geophysics*, *33*, 1004–1012.

Sebagenzi, M. N., G. Vasseur, and P. Louis (1992), Recent warming in central Zaire (Central Africa) inferred from disturbed geothermal gradients, *Palaeogeogr. Palaeoclimatol. Palaeoecol.*, *98*, 209–217.

Silliman, S. E., and D. F. Booth (1993), Analysis of time-series measurements of sediment temperature for identification of gaining v. losing portions of Juday Creek, *Indiana, J. Hydrol.*, *146*, 131–148.

Silliman, S. E., J. Ramirez, and R. L. McCabe (1995), Quantifying downflow through creek sediments using temperature time series: One-dimensional solution incorporating measured surface temperature, *J. Hydrol.*, *167*, 99–119.

Smith, L., and D. S. Chapman (1983), On the thermal effects of groundwater flow: 1. Regional scale systems, *J. Geophys. Res*, *88*, 593–608.

Stallman, R. W. (1960), Notes on the use of temperature data for computing ground-water velocity, *Tech. Rep. 3* (*Question 1*), Soc. Hydrotech. de Fr., Nancy, France.

Stallman, R. W. (1965), Steady one-dimensional fluid flow in a semi-infinite porous medium with sinusoidal surface temperature, *J. Geophys. Res.*, *70*, 2821–2827.

Stolk, P. (2000), Analysis of temperature measurements in the Dutch subsurface (20–300 m below ground surface) in relation to hydrological and meteorological conditions in the present and the past (in Dutch), Msc-thesis, Vrije Univ., Amsterdam.

Stuurman, R. J., and R. H. Atari (1997), The groundwater flow situation around the "Wijstgronden" near the village of Uden (in Dutch), *Tech. Rep. 97–212 (a)*, Neth. Inst. of Appl. Geosci. (NITG-TNO), Utrecht, Netherlands.

Taniguchi, M. (1993), Evaluation of vertical groundwater fluxes and thermal properties of aquifers based on transient temperature-depth profiles, *Water Resour. Res.*, *29*, 2021–2026.

Taniguchi, M., J. Shimada, T. Tadashi, I. Kayane, Y. Sakura, Y. Shimano, S. Dapahh-Siakwan, and S. Kawashima (1999a), Disturbances of temperature-depth profiles due to surface climate change and subsurface water flow: 1. An effect of linear increase in surface temperature cause by global warming and urbanization in the Tokyo metropolitan area, Japan, *Water Resour. Res.*, *35*, 1507–1517.

Taniguchi, M., D. R. Williamson, and A. J. Peck (1999b), Disturbances of temperature-depth profiles due to surface climate change and subsurface water flow: 2. An effect of step increase in surface temperature caused by forest clearing in southwest Western Australia, *Water Resour. Res.*, *35*, 1519–1529.

Van Balen, R., J. M. Verweij, J. D. van Wees, H. Simmelink, F. Van Bergen, and H. Pagnier (2002), Deep subsurface temperatures in the Roer Valley Graben and the Peelblock, the Netherlands—New results, *Geol. Mijnbouw*, *81*, 19–27.

Wallbraun, A. (1992), The impact of block-bounding faults on groundwater discharge in the Lower-Rhine Embayment (in German), Ph.D. thesis, Rheinisch-Westfälischen Tech. Hochsch., Aachen, Germany.

Woodbury, A. D., and L. Smith (1988), Simultaneous inversion of hydrogeologic and thermal data: 2. Incorporation of thermal data, *Water Resour. Res.*, *24*, 356–372.

Ziegler, P. A. (1994), Cenozoic rift system of western and central Europe: An overview, *Geol. Mijnbouw*, *73*, 99–127.

V. F. Bense and H. Kooi, Department of Hydrology and Geo-Environmental Sciences, Faculty of Earth and Life Sciences, Vrije Universiteit Amsterdam, de Boelelaan 1085, NL-1081 HV Amsterdam, Netherlands. (victor.bense@falw.vu.nl)